Am J Cancer Res 2022;12(5):2310-2322
www.ajcr.us /ISSN:2156-6976/ajcr0141770

Original Article

Atractylon inhibits the tumorigenesis of glioblastoma through SIRT3 signaling

Shanshan Sun[1,2*], Jiali Shi[1,2*], Xin Wang[1,2], Changgang Huang[1,2], Yuqian Huang[1,2], Jiayun Xu[1,2], Yuanyuan Jiang[1,2], Liying Cao[1], Tian Xie[1,2], Yongjie Wang[1,2], Zhihui Huang[1,2]

[1]*School of Pharmacy, Department of Neurosurgery, The Affiliated Hospital, Hangzhou Normal University, Hangzhou 311121, Zhejiang, China;* [2]*Key Laboratory of Elemene Class Anti-Cancer Chinese Medicines, Engineering Laboratory of Development and Application of Traditional Chinese Medicines, Collaborative Innovation Center of Traditional Chinese Medicines of Zhejiang Province, Hangzhou Normal University, Hangzhou 311121, Zhejiang, China.* [*]*Equal contributors.*

Received January 15, 2022; Accepted April 30, 2022; Epub May 15, 2022; Published May 30, 2022

Abstract: Glioblastoma (GBM) is the most common primary malignant brain tumor. Although there are various treatments for glioblastoma including surgery, radiotherapy, systemic therapy (chemotherapy and targeted therapy) and supportive therapy, the overall prognosis remains poor and the long-term survival rate is very low. Atractylon, a bioactive compound extracted from the Chinese herb *Atractylodes lancea* (Thunb.) DC. or *Atractylodes chinensis* (DC.) Koidz., has been reported to induce apoptosis and suppress metastasis in hepatic cancer cells. However, the roles and mechanisms of atractylon in GBM cells remain unknown. In the present study, we aimed to evaluate the effects of atractylon on the anti-tumorigenesis properties of GBM. Firstly, results of CCK8, colony formation, cell proliferation, and flow cytometry assays showed that atractylon inhibited the proliferation of GBM cells by arresting cells at the G1 phase of cell cycle. In addition, atractylon suppressed the migration and induced apoptosis of GBM cells. Mechanistically, atractylon treatment caused a significant up-regulation of sirtuin 3 (SIRT3, a tumor suppressor) mRNA and protein in GBM cells. Furthermore, inhibition of SIRT3 by the selective SIRT3 inhibitor 3-(1H-1,2,3-triazol-4-yl) pyridine (3-TYP) partially restored the anti-proliferation and migration effects of atractylon in GBM cells. Finally, atractylon treatment also inhibited the *in vivo* growth of GBM cells in xenograft models through SIRT3 activation. Taken together, these results reveal a previously unknown role of atractylon in inhibiting GBM *in vitro* and *in vivo* through up-regulating SIRT3, which suggests novel strategies for the treatment of GBM.

Keywords: Atractylon, tumorigenesis, glioblastoma, proliferation, migration, apoptosis, SIRT3

Introduction

Glioblastoma (GBM; WHO grade IV) is the most frequent and malignant brain tumor and typically associated with dismal prognosis and poor quality of life [1]. Currently, long-standing treatment options for glioblastoma include surgery, radiotherapy and temozolomide (TMZ) chemotherapy. TMZ is still the first-line chemotherapeutic drug for glioblastoma even though resistance is always identified after treatment, because other effective drugs are still not available [2, 3]. Furthermore, observed survival rates were 42.4% at 6 months, 17.7% at 1 year, and 3.3% at 2 years [4]. Thus, exploration of novel therapeutic drugs for glioblastomas is urgently needed.

In recent years, the naturally occurring products or their derivatives have become an important source of discovering and developing new anticancer drugs [5-7]. Atractylon (ATR) is a sesquiterpenoid extracted from *Atractylodes lancea* (Thunb.) DC. or *Atractylodes chinensis* (DC.) Koidz., and described as a basic component of antiviral, anti-inflammatory, hepatoprotective, and anticancer agent [8]. Previous studies have demonstrated that atractylon treatment prevents cognitive dysfunction, which induced by sleep -disorder-associated breathing issues by inhibiting chronic intermittent hypoxia-induced M1 microglial activation [9]. The protective effect of atractylon against oxidative stress induced by tert-butyl hydroperoxide is via its ability to quench free radicals [10]. Moreover, atrac-

tylon is also considered a promising natural agent for treating hepatic cancer by inhibiting cell proliferation, inducing apoptosis, and blocking invasion *in vitro* and cancer growth *in vivo* [11]. However, the roles of atractylon in GBM cells remain unclear.

Sirtuins (SIRTs) are a family of NAD^+-dependent deacetylases that regulate signaling pathways involved in cellular proliferation and differentiation, metabolism, stress response, and cancer [12, 13]. SIRT3 is synthesized as a 44-kDa polypeptide with an N-terminal targeting signal sequence for its mitochondrial localization. Under stress conditions, SIRT3 is translocated to the mitochondrial matrix, where proteolytic cleavage, yields the 28-kDa active form [14-16]. SIRT3 has been shown as a tumor suppressor in breast cancer [17], leukemia [18] and hepatocellular carcinoma [19-21]. Additionally, SIRT3 can induce cell arrest and apoptosis by regulating proteins such as Bcl-2, p53 and HIF-1α [18, 22-24]. Tumors lacking SIRT3 grow faster and have greater volume than control tumors in xenograft models [25]. Taken together, SIRT3 expression correlates with good outcomes and an increase in the overall survival of cancer patients. However, it remains unknown whether atractylon has any anti-glioma effects through activating SIRT3 signaling.

In the present study, we examined the effects of atractylon on the proliferation, migration and apoptosis of GBM cell lines C6 and DBTRG. We found that atractylon inhibited GBM cell proliferation by arresting cells at G1 phase of the cell cycle. Furthermore, atractylon induced the apoptosis and migration of GBM cells. Finally, we linked atractylon's anti-GBM effects with the activation of SIRT3 signaling both *in vitro* and *in vivo*. Altogether, our results demonstrate that the natural product atractylon exerts its anticancer effects on GBM cells through activating SIRT3 signaling.

Materials and methods

Cell culture and animals

The glioma cell lines C6 and DBTRG were kindly provided by Prof. Maojin Yao (Sun Yat-Sen University) and cultured in Dulbecco's Modified Eagle's Medium supplement with 10% FBS (Gibco) and 1% penicillin/streptomycin (Gibco) in an atmosphere of 95% air and 5% CO_2 at 37°C. BALB/C nude male mice (18-22 g, 6-8 weeks) were purchased from Shanghai SLAC Laboratory Animal Co., Ltd. (Shanghai, China). The mice were housed in a standard laboratory condition (temperature 22±2°C and humidity 50-60%) at Laboratory Animal Center of Hangzhou Normal University. The Animal Care and Use Committee of Hangzhou Normal University approved all of the mouse protocols.

Drugs

Atractylon was purchased from Beijing Solarbio Science & Technology Co., Ltd. (#SA9810, Beijing, China) and Shanghai yuanye Bio-Technology Co., Ltd. (#B20129, Shanghai, China). A stock solution of 500 mM was prepared in Dimethyl sulfoxide (D8371, Solarbio) and stored at -80°C. 3-TYP was purchased from MedChemExpress LLC (#HY-108331) with a stock solution of 500 mM prepared in Dimethyl sulfoxide and stored at -80°C.

CGGA database analysis

The Chinese Glioma Genome Atlas (CGGA) (http://www.cgga.org.cn) was an online database for analyzing brain tumors datasets from Chinese cohorts. This database was used to browse *SIRT3* mRNA expression profile and to perform survival analysis in all grade gliomas. The hazard ratio with 95% confidence intervals and logrank *p*-value were also computed.

Molecular docking simulation

The 3D structure of SIRT3 (PDB: 3GLS) was obtained from the Protein Data Bank (http://www.rcsb.org/pdb). The 3D structure of atractylon was obtained from a database of chemical modules (http://pubchem.ncbi.nlm.nih.gov). After SIRT3 and atractylon were imported into Discovery Studio (BIOVIA), the water molecules in SIRT3 were removed, whereas all hydrogen atoms were added to the SIRT3 file according the "Prepare Protein" function at PH 6.9, temperature 25°C. Then, the atractylon structure was minimized by the algorithm of smart minimizer. The atractylon structure was optimized according the "Prepare Ligands" function at PH 6.9. Finally, the optimal structures of SIRT3 and atractylon were given to the CHARMm force field. The docking site was defined from the recorded active site. Interactions between the identified atractylon and pro-

tein structure of 3GLS were observed in the software Discovery Studio 2019.

Cell viability assays

Cell viability was detected by the CCK-8 cell counting kit (A311-01/02, Vazyme Biotech). Briefly, cells were seeded into 96-well plates at a density of approximately 3,000 cells per well and cultured for 24 h. Then they were starved for 24 h in serum free media followed by incubation with different concentrations of atractylon, and cultured for another 24 h. Subsequently, 10 μL CCK-8 solution was added to each well and incubated at 37°C for 2 h. The optical density of cells was measured at the wavelength of 450 nm using a microplate reader (Varioskan Flash, Thermo scientific, USA).

Cell cycle assays

After treatment with 100 μM atractylon for 24 h, cell cycle was measured using the Cell Cycle Staining Kit (#A01031, MULTI SCIENCES, Hangzhou, China) following the manufacturer's instructions. Briefly, cells were re-suspended and mixed in DNA staining solution. After incubation for 30 min, cell cycle was detected with a flow cytometer (CytoFLEX S, Beckman Coulter). The results were presented as percentage of cells at each phase of the cell cycle.

Apoptosis assays

Cell apoptosis was measured using the Annexin V-FITC/PI Apoptosis Detection Kit (#A00947, MULTI SCIENCES, Hangzhou, China) following the manufacturer's instructions after treatment with 100 μM atractylon for 24 h. Briefly, cells were re-suspended and mixed in 500 μL PI. After incubation for 15 min, cell apoptosis was detected with a flow cytometory (CytoFLEX S, Beckman Coulter).

Colony formation analysis

The C6 and DBTRG cell suspensions were plated in a 6-well culture plate at 5×10^2 cells/well and grown for 12 h. The supernatants were removed and fresh media containing atractylon at the final concentration of 100 μM were added. The cells were cultured for 7 d at 37°C. Finally, the supernatants were removed and the cells were washed with PBS twice. Then the colonies were fixed with 4% paraformaldehyde (PFA) for 15 min at RT, and then stained with crystal violet solution (0.1%) for 30 min. After the staining solution was removed, the colonies were washed with PBS and the plate placed upside down on absorbent papers to blot dry, followed by air drying or drying at 37°C. After 0.5 mL of 33% acetic acid was added to each well for decolorization, was detected absorbance at 570 nm using a microplate reader (Varioskan Flash, Thermo scientific, USA) after sufficient vibration.

Transwell and wound-healing assays

For the transwell migration assay, 100 μL cells at the concentration of 1×10^5/mL were suspended in the upper chamber of a 24-well transwell plate. After 24 h of co-culturing, the cells were fixed, stained, and counted under a Nikon light microscope (Nikon Corporation Ci-S). For the wound-healing assay, a monolayer of cells at 95% confluence was scratched with a sterile plastic tip (diameter: 4 mm) and then cultured in serum-free medium.

Western blotting

Cultured cells or tumor tissues from the xenograft models were lysed in ice-cold RIPA Buffer (R0010, Solarbio) at 4°C for 30 min and centrifuged at 1,4000 g for 20 min. After quantification with the BCA method, proteins were mixed with 5× loading buffer and boiled at 100°C for 15 min. The protein samples were then separated using 10-12% sodium dodecyl sulphate-polyacrylamide gel electrophoresis (SDS-PAGE) and transferred onto PVDF membranes. After blocking in TBST containing 5% skim milk for 1 h at RT, the immunoblots were incubated with different primary antibodies at 4°C overnight. Primary antibodies used included rabbit anti-p53 (#2527, CST, 1:1,000), rabbit anti-cleaved caspase-3 (#9661, CST, 1:1,000), rabbit anti-Lamin B1 (#ab16048, Abcam, 1:1,000), rabbit anti-SIRT3 (#10099-1-AP, Proteintech, 1:1,000), rabbit anti-Cyclin D1 (#55506, CST, 1:1,000), mouse anti-*β*-actin (#200068-8F10, ZEN BIO, 1:5,000) or mouse anti-*β*-tubulin (200608, ZEN BIO, WB 1:5,000) as a loading control was detected alongside the experimental samples. Subsequently, the membranes were washed three times in TBST, and incubated with the horseradish peroxidase (HRP)-conjugated secondary antibodies [1:10,000, Sigma, A0545 (goat anti-rabbit), A9044 (goat anti-mouse)] for

1 h. After being washed in TBST for another three times, protein signals were detected using the ECL detection kit (Biomedical Technology). Blots were analyzed using the ImageJ software.

RNA extraction and quantitative real-time PCR (qRT-PCR)

Total RNA was extracted by the RNA-Quick Purification Kit (YISHAN Biotechnology, ES-RN001) according to the manufacturer's protocol. RNA content was quantified by the Thermo Scientific™ NanoDrop™ One. cDNA synthesis was performed with the cDNA DyNAmo Kit (Vazyme, R211-01/02). qPCR was performed with the SYBR Green PCR master mix (Vazyme, Q511-02/03). PCR real time cycling conditions were programmed as such: first step (95°C, 15 min), cycling step (denaturation 94°C, 15 s, annealing at 56°C or 60°C for 30 s, and final extension at 72°C for 30 s×40 cycles). This was followed by a melting curve analysis to confirm the specificity of the primers. The CT value was corrected by the corresponding-actin control CT values. The primers used in this study were synthesized by Shanghai Sangon Biotech: *SIRT3*, 5'-CATGAGCTGCAGTGACTGGT-3' and 5'-GAGCTTGCCGTTCAACTAGG-3'; β-actin, 5'-AGACTTCGAGCAGGAGATGGC-3' and 5'-TCGTTGCCAATAGTGATG-ACCTG-3'.

Immunofluorescent analysis

Cultured cells were rinsed once with PBS, fixed in 4% PFA for 20 min. Then, the cells were blocked and permeabilized with 0.1% Triton X-100 in PBS containing 5% normal goat serum (NGS) at room temperature for 1 h. Subsequently, the cells were incubated with primary antibodies at 4°C overnight, washed three times in PBS and then with secondary antibodies at room temperature for 1 h. The primary antibodies included rabbit anti-SIRT3 (#10099-1-AP, Proteintech, 1:500), mouse anti-PH3 (ab14955, Abcam, 1:2,500). After being washed in PBS for another three times, cells were mounted. Images were acquired using a fluorescence microscopy (Olympus VS200).

In vivo glioma models and atractylon administration

A total of 3×10^6 C6 cells were resuspended in serum-free DMEM medium and inoculated subcutaneously into nude mice. When the visible tumors at the injection sites grew to 50-100 mm^3, the mice were randomly divided into two groups: the vehicle control group and the atractylon group. Atractylon was dissolved in corn oil and given to the mice by intragastric administration at 20 mg/kg, which dosed at 0.1 mL/10 g of body weight for 23 d. Corn oil alone was given as a control. In the end, the mice were sacrificed by cervical dislocation, the tumors, hearts, livers, lungs, and kidneys were collected. The tumors were photographed and weighed immediately. Then the tumors and organs were fixed in 4% PFA and subjected to HE analysis.

Statistical analysis

All data values were presented as mean ± SEM derived from at least three independent experiments. The GraphPad Prism 8.0.1 software was used for statistical analysis. For comparison between two groups, we used unpaired t test; for comparison between four groups, we used the Turkey or Kruskal-Wallis test. For the cell viability assays and **Figure 5**, we used one-way ANOVA. A *P*-value of < 0.05 was considered statistically significant.

Results

Atractylon decreased the viability and inhibited the proliferation of GBM cells in vitro

To observe the cytotoxicity and inhibitory effects of atractylon in GBM cells, the GBM C6 and DBTRG cell lines were treated with different concentrations of atractylon for different times. Cell counting kit-8 (CCK8) assays showed that atractylon treatment significantly decreased the viability of both C6 and DBTRG cells in dose and time-dependent manners (**Figure 1A**, **1B**). To further determine whether the reduced viability of GBM cells by atractylon was due to the decreased ability of cell proliferation, a colony-formation assay was performed. As shown in **Figure 1C**, **1D**, atractylon treatment notably suppressed the colony-formation efficiency of both C6 and DBTRG cells as expected. Furthermore, PH3 (a cell marker of proliferation) staining also showed that the percentages of $PH3^+$ cells obviously decreased in both C6 and DBTRG cells treated with atractylon (**Figure 1E**, **1F**). Consequently, these results revealed that atractylon suppressed the viability and inhibited the proliferation of GBM cells *in vitro*.

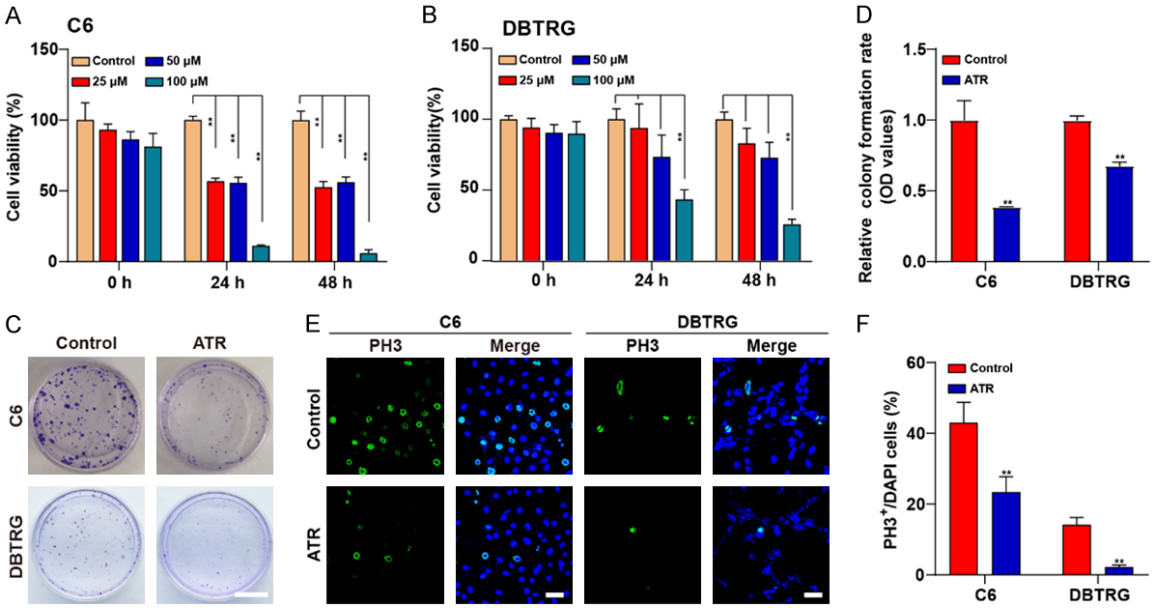

Figure 1. Atractylon decreased the viability and inhibited the proliferation of GBM cells *in vitro*. (A) The viability of C6 cells treated with different atractylon concentrations as determined by CCK8 assays (n=5 per group). (B) The cell viability of DBTRG cells treated with different atractylon concentrations as determined by CCK8 assays (n=5 per group). (C) Representative images of C6 and DBTRG cells treated with 100 μM atractylon for 7 d in colony formation assays. Scale bar, 10 mm. (D) Quantitative analysis of the CV-stained colonies dissolved in 33% acetic acid and measured by absorbance at 570 nm as shown in (C) (n=4 per group). (E) Immunostaining of PH3 (green) in C6 and DBTRG cells treated with 100 μM atractylon for 24 h. Scale bar, 50 μm. (F) Quantitative analysis of the percentages of PH3-positive cells over total C6 and DBTRG cells in one field as shown in (E) (n=6 per group). Data were mean ± SEM. $^{*}P < 0.05$, $^{**}P < 0.01$.

Atractylon caused G1 cell cycle arrest and induced apoptosis in GBM cells

To determine whether atractylon inhibited the proliferation of GBM cells by inducing cell cycle arrest, flow cytometry analysis was carried out. As shown in **Figure 2A**, **2B**, the proportion of C6 cells in the G1 phase significantly increased after atractylon treatment, compared with control cells, resulting in decreased number of C6 cells in the G2/M and S phases. We next examined the expression of cyclin D1 after atractylon treatment in C6 cells since it is a key protein that regulates the G1 phase of cell cycle and essential for cell cycle regulation [26]. As predicted, cyclin D1 expression was indeed decreased in atractylon-treated C6 cells (**Figure 2G**, **2J**). In addition, previous studies have shown that activated P53 causes a variety of responses including cell cycle arrest and apoptosis [27-31]. As shown in **Figure 2G**, **2H**, the expression of P53 increased in atractylon-treated C6 cells. Taken together, these results illustrated that atractylon treatment caused G1 arrest through downregulating cyclin D1 expression, which resulted in cell proliferation inhibition of GBM cells.

We next examined the effects of atractylon on GBM cell apoptosis by flow cytometry assays, PI staining, and western blotting. As shown in **Figure 2C**, **2D**, normal healthy cells that were not stained were shown in the lower left region, and early apoptotic cells stained by Annexin V-FITC only were in the lower right part region, while necrotic and late apoptotic cells that stained by both Annexin V-FITC and PI were shown in the upper right region. Our data showed that atractylon treatment dramatically induced the apoptosis of C6 cells (**Figure 2C**, **2D**). Imaging results of PI staining also showed that atractylon treatment significantly promoted the apoptosis of C6 cells (**Figure 2E**, **2F**). To further confirm these findings, the expression of apoptosis-associated proteins such as cleaved caspase-3 was also examined in C6 cells. As shown in **Figure 2G**, **2I**, the expression of the pro-apoptotic factor cleaved caspase-3 was significantly upregulated in atractylon-treated C6 cells. Taken together, these results indicated

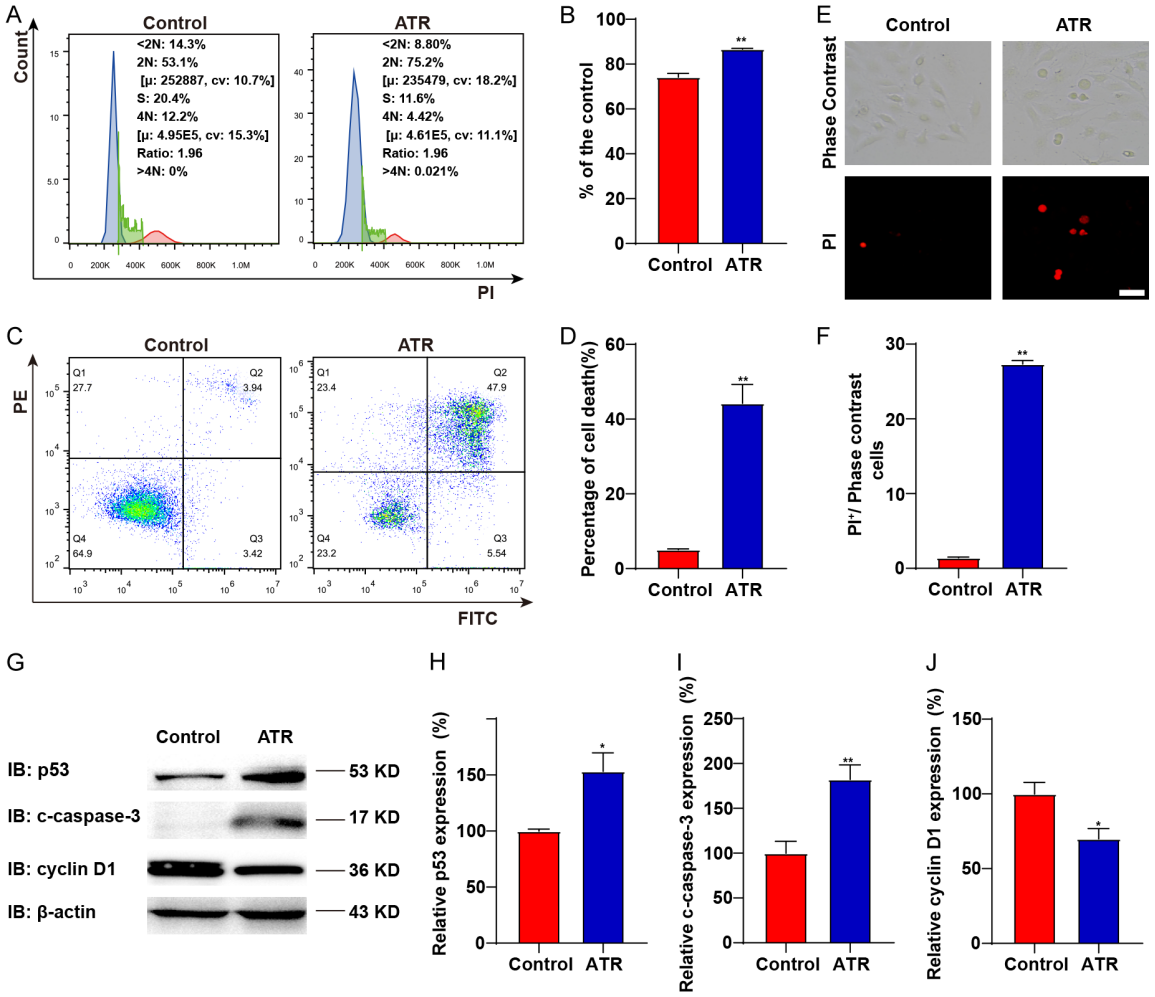

Figure 2. Atractylon caused G1 cell cycle arrest and induced apoptosis in GBM cells. (A) Flow cytometric analysis of cell cycle distribution of C6 cells treated with 100 μM atractylon for 24 h (n=4 per group). (B) Quantitative analysis of the percentage of 2n-phase C6 cells as shown in (A). (C) Flow cytometric analysis of annexin V/FITC/PI stained control and treated (100 μM atractylon for 24 h) C6 cells. (D) Quantitative analysis of the apoptosis rate of C6 cells as shown in (C) (n=4 per group). (E) Representative image of PI staining in C6 cells after treatment with vehicle control or 100 μM atractylon for 24 h. Scale bar, 200 μm. (F) Quantitative analysis of the percentage of PI^+ cells in total cells in one field as shown in (E) (n=4 per group). (G) The expression of P53, cleaved caspase-3, and cyclin D1 in treated (100 μM atractylon for 24 h) C6 cells was detected by western blot. (H-J) Quantitative analysis of P53 (H), cleaved caspase-3 (I), and cyclin D1 (J) levels as shown in (G) (n=3 per group). Data were mean ± SEM. $^*P < 0.05$, $^{**}P < 0.01$.

that atractylon treatment induced GBM cell apoptosis.

Atractylon inhibited the migration of GBM cells

To examine whether atractylon affects GBM cell migrations, the scratch migration assay was performed. After the wound was introduced the confluent monolayer of C6 or DBTRG cells was treated with control or atractylon for 24 and 48 hours. As shown in **Figure 3A-C**, atractylon treatment markedly inhibited the migration of C6 and DBTRG cells, compared with that in controls. To further verify the effect of atractylon on migration of GBM cells, transwell assays were performed. As shown in **Figure 3D-F**, C6 and DBTRG cells were allowed to migrate for 24 hours in the presence or absence of atractylon in the lower chamber. In the control group, both cell lines migrated through the filter after being cultured for 24 hours while the number of migrating cells significantly decreased in the atractylon treatment group. Taken together, these results revealed that atractylon treatment inhibited the migration of GBM cells.

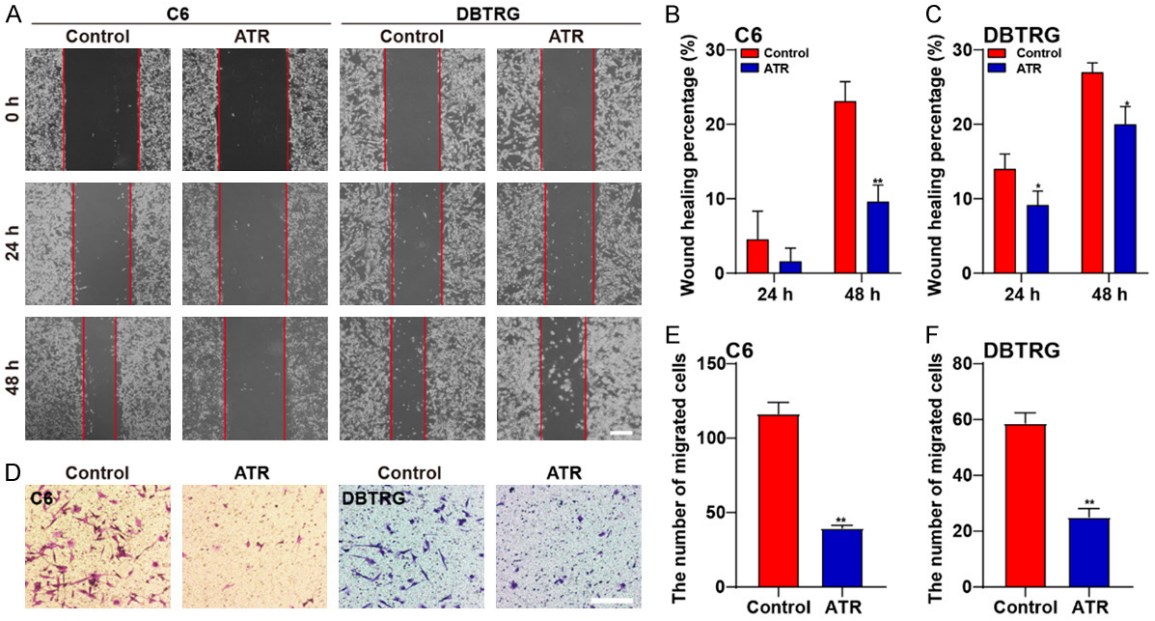

Figure 3. Atractylon inhibited the migration of GBM cells. (A) Representative images from three independent experiments of C6 and DBTRG cells treated with 100 μM atractylon in wound healing assays. Phase-contrast images were acquired at 0, 24 and 48 h after scratching. (B, C) Quantitative analysis of the relative wound healing area (normalized to 0 h) (n=20 per group). Scale bar, 900 μm. (D) Representative images of C6 and DBTRG cells treated with 100 μM atractylon for 24 h in transwell migration assays. Scale bar, 100 μm. (E, F) Quantitative analysis of the number of migrated C6 cells (E) or DBTRG cells (F) as shown in (D, n=6 per group). Data were mean ± SEM. $^{*}P < 0.05$, $^{**}P < 0.01$.

Atractylon inhibited cell proliferation and migration via activating SIRT3 signaling in vitro

Previous studies have shown that atractylon treatment promoted SIRT3 expression [9] and SIRT3 functions as a tumor suppressor in certain types of cancers such as breast cancer [17]. According to survival analysis based on the Chinese Glioma Genome Atlas database (CGGA database, http://www.cgga.org.cn/), the survival time of glioma patients with lower SIRT3 expression was noticeably shorter, suggesting that SIRT3 expression might be a prognostic marker in glioma patients (**Figure 4A**, **4B**). Homoplastically, molecular docking was used to predict whether SIRT3 and atractylon have binding sites. The binding situation and sites of SIRT3 and atractylon were shown in **Figure 4C**, **4D** by using Discovery Studio. Next, we investigated whether atractylon inhibited the GBM tumorigenesis through activating SIRT3 signaling. As predicted, western blotting showed that the protein level of SIRT3 increased significantly in C6 cells treated with atractylon (**Figure 4E-G**). Furthermore, immunostaining also showed significantly increased SIRT3 signal intensity in these atractylon-treated C6 cells (**Figure 4H**, **4I**). qPCR showed the mRNA level of *SIRT3* was elevated in the atractylon-treated C6 cells as well (**Figure 4J**), which indicates that SIRT3 was upregulated at both the transcriptional and translational level by atractylon. Taken together, these results indicated that atractylon treatment upregulated the expression of SIRT3 in GBM cells, which contribute to the inhibition of GBM cell tumorigenesis.

To further explore the roles of SIRT3 in atractylon-induced inhibition of GBM tumorigenesis, 3-TYP, a selective SIRT3 inhibitor [32-34] was employed. As hypothesized, the application of 3-TYP before atractylon incubation partially rescued the inhibition of cell proliferation in CCK8 assays (**Figure 5A**, **5B**), colony formation analysis (**Figure 5C**, **5D**), and PH3 immunostaining (**Figure 5E**, **5F**) in atractylon-treated C6 cells. Meanwhile, 3-TYP pretreatment also restored the inhibition of migration in atractylon-treated C6 cells (**Figure 5G**, **5H**). In addition, western blotting showed that the protein level of SIRT3, P53 and cleaved caspase-3 were also partially decreased in C6 cells (**Figure 5I-L**).

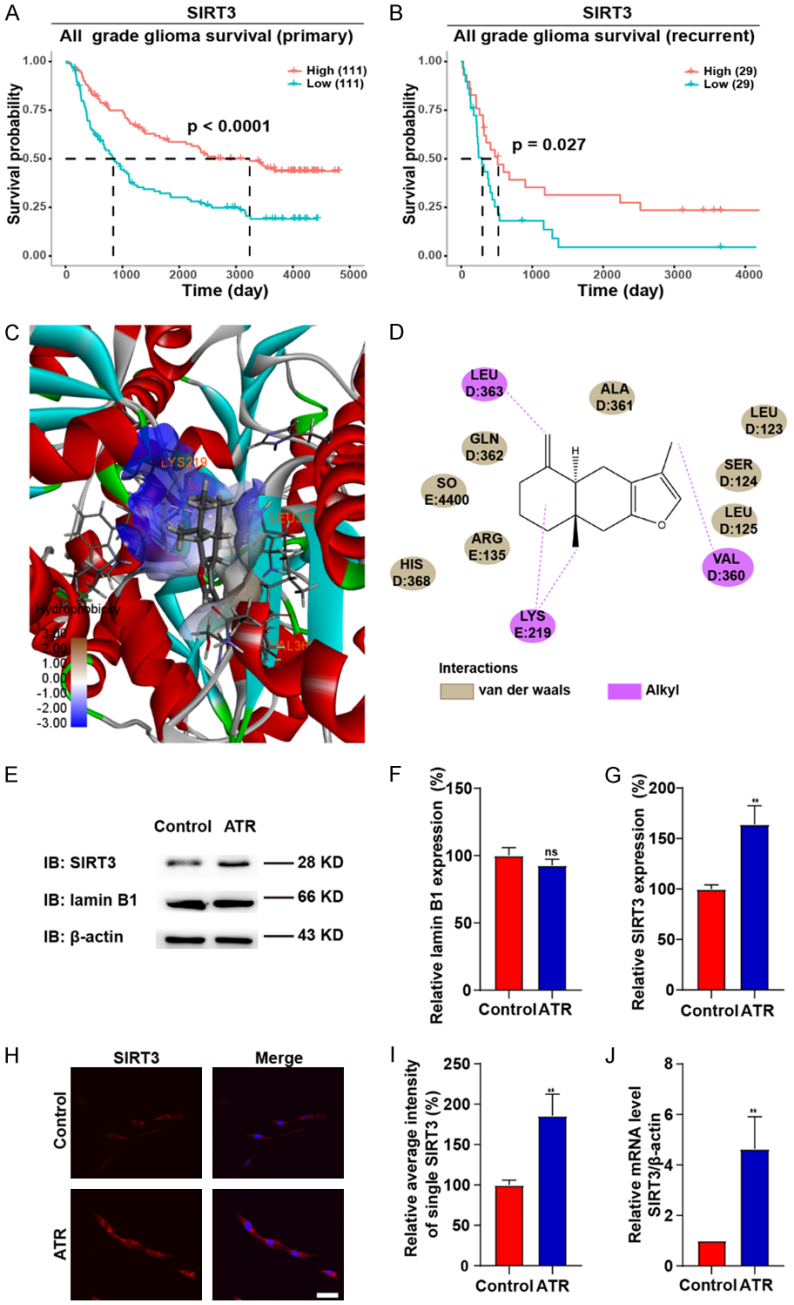

Figure 4. Atractylon treatment upregulated SIRT3 expression in C6 cells. (A, B) Survival analysis of SIRT3 expression in all primary (A) and recurrent (B) grade glioma. (C) 3D docking mode between atractylon and SIRT3 based on Discovery Studio assimilation and active site-amino acids (Leu 363, Lys, 219, and Val 360). (D) 2D diagram of the predicted interactions between atractylon and SIRT3; backbone of the protein is colored in grey. Ligand-protein interactions are colored depending on their type: alkyl is colored in purple, conventional hydrogen bonds are colored in brown. (E) The expression of SIRT3 and Lamin B1 in C6 cells treated with 100 μM atractylon for 24 h was detected by western blot. (F, G) Quantitative analysis of the relative SIRT3 (G) and Lamin B1 (F) levels as shown in (E) (n=3 per group). (H) Immunostaining of SIRT3 (red) in C6 cells treated with 100 μM atractylon for 24 h. (I) Quantitative analysis of the relative average fluorescence intensity of SIRT3 in single C6 cell as shown in (H) (n=6 per group). Scale bar, 25 μm. (J) qPCR analysis results of *SIRT3* mRNA levels in C6 cells treated with atractylon at 100 μM for 24 h (n=4 per group). Data were mean ± SEM. $^{*}P < 0.05$, $^{**}P < 0.01$.

Taken together, these results strongly implied that atractylon inhibited the tumorigenesis of GBM cells by activating SIRT3 signaling *in vitro*.

Atractylon inhibited the tumorigenesis of GBMs by activating SIRT3 signaling in vivo

In view of *in vitro* experiments showing atractylon's significant anti-GBM activities, we further confirmed the effect of atractylon in xenograft glioma models. A subcutaneous glioblastoma tumor mouse model was established, who received intragastric administration of atractylon at the dose of 20 mg/kg/day for 23 days. As shown in **Figure 6A**, **6B**, tumors from atractylon-treated mice were obviously smaller than those in the control group, and the tumor weight was significantly reduced in atractylon-treated nude mice, compared with control group. Additionally, consistent with the *in vitro* results, the expression of SIRT3, P53, and cleaved caspase-3 also significantly increased (**Figure 6C-F**). Furthermore, PH3 staining also showed that the proliferation of these tumors was significantly inhibited after atractylon treatment (**Figure 6G**). To assess the *in vivo* side effects of atractylon, various organs were harvested, sectioned, and stained with HE. No histological differences in the lung, heart, liver, spleen, or kidney were found between the control and atractylon-treated mice, indicating an

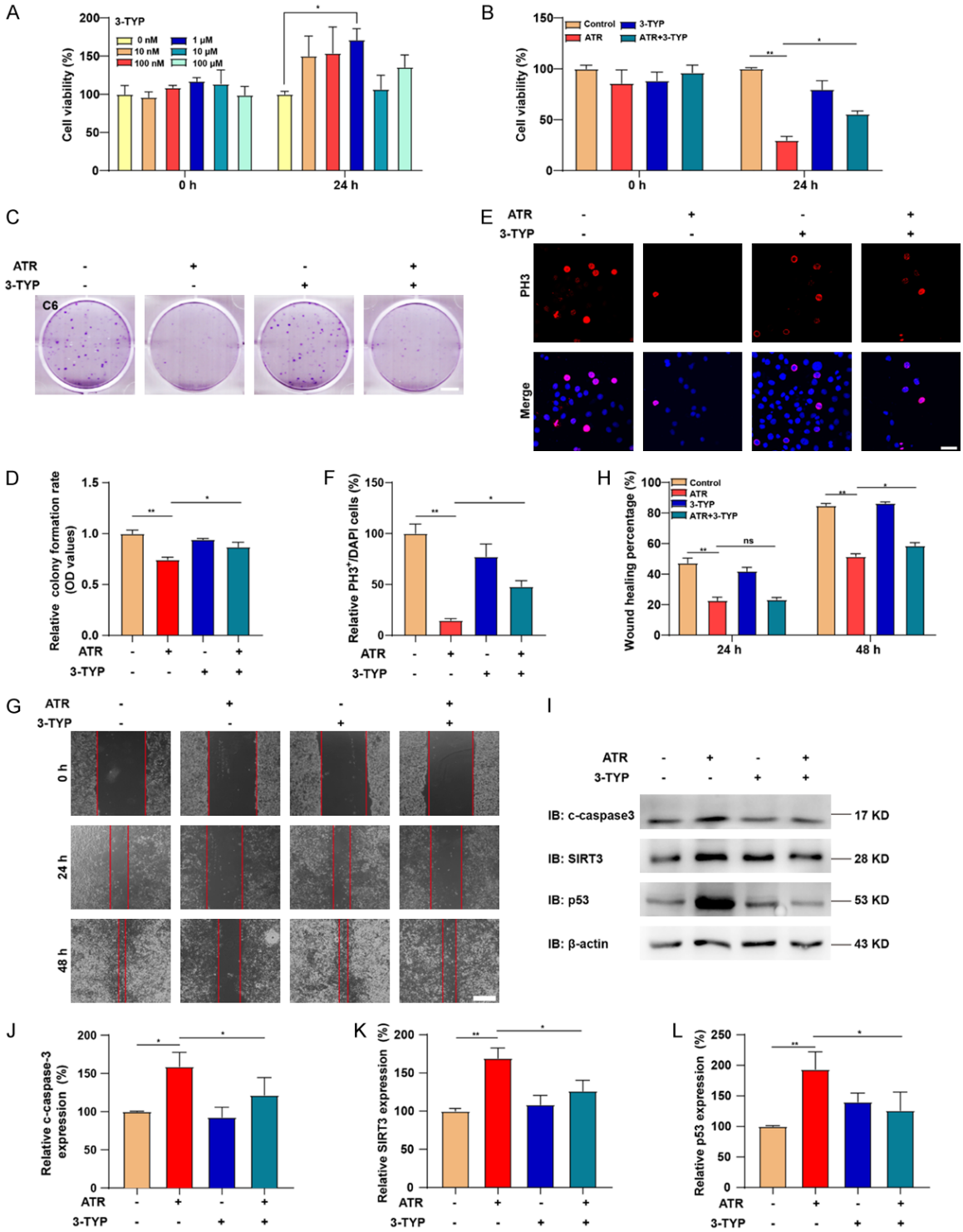

Figure 5. Atractylon inhibited C6 cell proliferation and migration via activating SIRT3 signaling *in vitro*. (A) The viability of C6 cells treated with different 3-TYP concentrations was determined by CCK8 assays (n=5 per group). (B) The viability of C6 cells treated with atractylon and 3-TYP was determined by CCK8 assays (n=5 per group). (C) Colony formation assays detecting the proliferation of C6 cells respectively treated with 100 μM atractylon for 24 h, 1 μM 3-TYP for 24 h, and 100 μM atractylon and 1 μM 3-TYP for 1 week. Scale bar, 700 mm. (D) Quantitative analysis of the surviving colonies as shown in (C) (n=3 per group). (E) Immunostaining of PH3 (red) in C6 cells with different treatment. Scale bar, 50 μm. (F) Quantitative analysis of the percentage of PH3 positive cells over total C6 cells in one filed as shown in (E) (n=6 per group). (G) Representative images from three independent experiments of C6 cells treated with vehicle control, 100 μM atractylon, 1 μM 3-TYP, or 100 μM atractylon and 1 μM 3-TYP in wound

healing assays. Phase-contrast images were acquired at 0, 24, and 48 h after scratching. Scale bar, 900 μm. (H) Quantitative analysis of the relative wound healing area as shown in (G). (I) The expression of SIRT3, P53, and cleaved caspase-3 in C6 cells treated with vehicle control, or 100 μM atractylon, 1 μM 3-TYP, 100 μM atractylon and 1 μM 3-TYP was detected by western blot. (J-L) Quantitative analysis of the relative levels of cleaved caspase-3 (J), SIRT3 (K) and p53 (L) as shown in (I) (n=3 per group). Data were mean ± SEM. $^{*}P < 0.05$, $^{**}P < 0.01$.

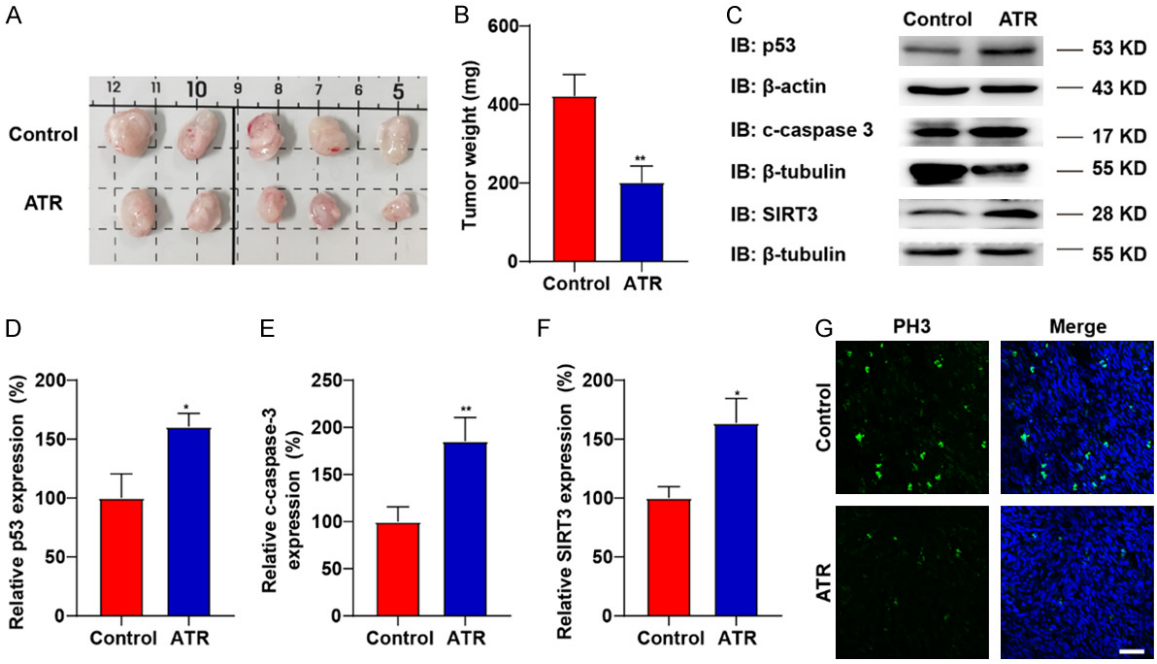

Figure 6. Atractylon inhibited the tumorigenesis of GBMs by activating SIRT3 signaling in *vivo*. (A) Representative images of C6 xenograft tumors after treatment with vehicle control or 20 mg/kg atractylon for 23 d. (B) Tumor weight in each group (n=10 per group). (C) The expression of P53, cleaved caspase-3, and SIRT3 in xenograft tumor tissues after treatment with vehicle control or 20 mg/kg atractylon for 23 d was detected by western blot. (D-F) Quantification of the relative levels of p53 (D), cleaved caspase-3 (E), and SIRT3 (F) as shown in (C) (n=3 per group). (G) Immunostaining of PH3 (green) in tumor tissues from mice treated with vehicle control or 20 mg/kg atractylon for 23 d. Scale bar, 50 μm. Data were mean ± SEM. $^{*}P < 0.05$, $^{**}P < 0.01$.

absence notable toxicity (Supplementary Figure 1). Taken together, these results suggested that atractylon inhibited the tumorigenesis of GBMs by activating SIRT3 signaling *in vivo* without notable side effects.

Discussion

In the present study, we found that atractylon could inhibit the proliferation and migration of GBM cells, and induce the apoptosis of GBM cells through activating SIRT3 signaling *in vitro* and *in vivo* (**Figure 7**). This study has identified an unrecognized role and mechanism of action for atractylon in anti-GBM and provided novel strategies for the treatment of GBMs.

Medicinal herbs have been used to treat various diseases under the guidance of traditional Chinese medicine theories for thousands of years in China. In recent decades, the natural products have become valuable resources for the discovery and development of new anticancer drugs. Previous studies have shown multiple activities for atractylon, such as anti-inflammatory, antinociceptive, antiviral, anti-ulcer, antitumor, and Na^{+}/K^{+}-ATPase inhibition activities [35-38]. Consistent with these findings, our *in vitro* and *in vivo* data showed that atractylon inhibited cell proliferation, induced G1 arrest, and suppressed the migration of GBM cells.

How does atractylon perform its anti-GBM function? SIRT3 is a key NAD^{+}-dependent protein deacetylase in the mitochondria of mammalian cells, functioning to prevent cell aging and transformation via the regulation of mitochondrial metabolic homeostasis. In addition, SIRT3 has been a major focus in the scientific community in the study of cancer, a leading

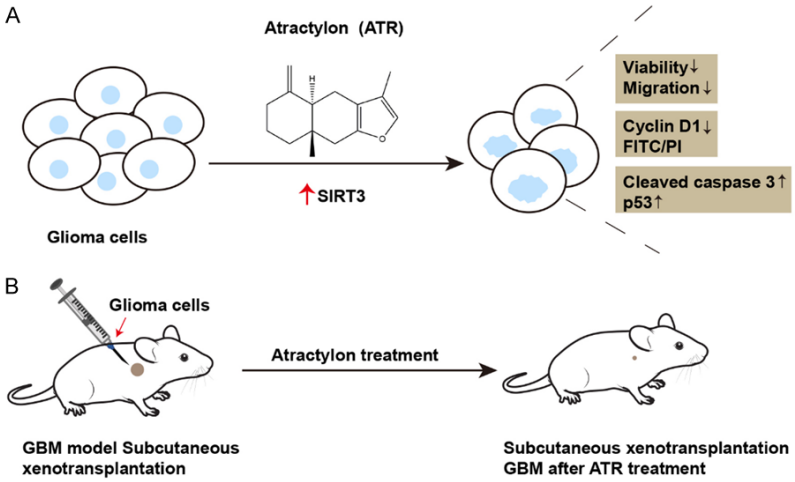

Figure 7. A working model of atractylon action on GBM cells. Atractylon treatment activates the expression of SIRT3 in GBM cells, which may in turn inhibit typical GBM tumorigenic characteristics, including blocking cell proliferation, suppressing cell migration, and inducing the apoptosis of GBM cells both *in vitro* and *in vivo*.

cause of death worldwide, as the role of SIRT3 is identified in the hallmark of cancer. With its central role in mitochondrial biology, SIRT3 contributes to cell survival by modulating oxidative stress pathways. In head and neck squamous cell carcinoma where SIRT3 is overexpressed, SIRT3 helps maintain ROS levels at appropriate levels to maintain the proliferative and aggressive phenotype, thus preventing apoptosis and promoting carcinogenesis [39]. Conversely, a pro-apoptotic role for SIRT3 in cancers has also been revealed. Treating chronic myelogenous leukemia K562 and promyelocytic human leukemia U937 cells with Kaempferol, a flavonoid with antioxidant and pro-oxidant activities present in various natural sources, can result in the inactivation of Akt and activation of the mitochondrial phase of the apoptotic program with an increase in Bax and SIRT3, decrease in Bcl-2, release of cytochrome c, activation of caspase-3, and cell death, suggesting a tumor suppressor role of SIRT3 [18]. In the present study, several lines of evidence showed that atractylon inhibited the tumorigenesis of GBMs by activating SIRT3 signaling *in vitro* and *in vivo*. Firstly, SIRT3 expression was increased sharply at both the mRNA and protein level in atractylon-treated GBM cells. Secondly, the SIRT3 inhibitor 3-TYP could partially restore the anti-tumor effects on GBM cells treated with atractylon. Thirdly, SIRT3 expression was increased dramatically in xenograft glioma models after atractylon treatment. How atractylon treatment can activate the SIRT3 signaling needs further exploration.

In summary, the present study has demonstrated that atractylon exerts significant anti-tumor effects by promoting SIRT3 expression *in vitro* and *in vivo*, and provided new insights for future research of atractylon in the treatment of GBM. To maximize the potential of atractylon for clinical applications, large-scale and multicenter collaborative clinical trials are urgently needed in the future.

Acknowledgements

This work was supported by the National Natural Science Foundation (92049104, 81801102 and 82071230), the Scientific Research Foundation for Scholars of HZNU (4125C5021920453 and 4125C50220204109), the patent (202111334909.7) and General scientific research project of Zhejiang Provincial Department of Education in 2021 (Y202147688).

Disclosure of conflict of interest

Zhihui Huang and Shanshan Sun are coauthors on a patent applied for by Hangzhou Normal University. This does not alter the authors' adherence to policies on sharing data and materials.

Abbreviations

ATR, Atractylon; GBM, Glioblastoma; SIRT3, Sirtuins 3; qPCR, Quantitative real-time PCR; 3-TYP, 3-(1H-1,2,3-triazol-4-yl) pyridine.

Address correspondence to: Tian Xie, Yongjie Wang and Zhihui Huang, School of Pharmacy, and Department of Neurosurgery, The Affiliated Hospital, Hangzhou Normal University, Hangzhou 311121,

Zhejiang, China. E-mail: tianxie@hznu.edu.cn (TX); wangyongjie@hznu.edu.cn (YJW); huang0069@hznu.edu.cn (ZHH)

References

[1] Ohgaki H and Kleihues P. The definition of primary and secondary glioblastoma. Clin Cancer Res 2013; 19: 764-772.

[2] Clarke J, Butowski N and Chang S. Recent advances in therapy for glioblastoma. Arch Neurol 2010; 67: 279-283.

[3] Lee SY. Temozolomide resistance in glioblastoma multiforme. Genes & Diseases 2016; 3: 198-210.

[4] Ohgaki H, Dessen P, Jourde B, Horstmann S, Nishikawa T, Di Patre PL, Burkhard C, Schüler D, Probst-Hensch NM, Maiorka PC, Baeza N, Pisani P, Yonekawa Y, Yasargil MG, Lütolf UM and Kleihues P. Genetic pathways to glioblastoma: a population-based study. Cancer Res 2004; 64: 6892-6899.

[5] Wu P, Dong XM, Song GQ, Wei MM, Fang C, Zheng FB, Zhao YJ, Lu HQ, Cheng LH, Zhou JL and Xie T. Bioactivity-guided discovery of quality control markers in rhizomes of Curcuma wenyujin based on spectrum-effect relationship against human lung cancer cells. Phytomedicine 2021; 86: 153559.

[6] Dong H, Wang M, Chang C, Sun M, Yang F, Li L, Feng M, Zhang L, Li Q, Zhu Y, Qiao Y, Xie T and Chen J. Erianin inhibits the oncogenic properties of hepatocellular carcinoma via inducing DNA damage and aberrant mitosis. Biochem Pharmacol 2020; 182: 114266.

[7] Wang X, Liu Z, Sui X, Wu Q, Wang J and Xu C. Elemene injection as adjunctive treatment to platinum-based chemotherapy in patients with stage III/IV non-small cell lung cancer: a meta-analysis following the PRISMA guidelines. Phytomedicine 2019; 59: 152787.

[8] Koonrungsesomboon N, Na-Bangchang K and Karbwang J. Therapeutic potential and pharmacological activities of Atractylodes lancea (Thunb.) DC. Asian Pac J Trop Med 2014; 7: 421-428.

[9] Lin Y, Liu X, Tan D and Jiang Z. Atractylon treatment prevents sleep-disordered breathing-induced cognitive dysfunction by suppression of chronic intermittent hypoxia-induced M1 microglial activation. Biosci Rep 2020; 40: BSR20192800.

[10] Hwang JM, Tseng TH, Hsieh YS, Chou FP, Wang CJ and Chu CY. Inhibitory effect of atractylon on tert-butyl hydroperoxide induced DNA damage and hepatic toxicity in rat hepatocytes. Arch Toxicol 1996; 70: 640-644.

[11] Cheng Y, Chen T, Yang X, Xue J and Chen J. Atractylon induces apoptosis and suppresses metastasis in hepatic cancer cells and inhibits growth in vivo. Cancer Manag Res 2019; 11: 5883-5894.

[12] Haigis MC, Deng CX, Finley LW, Kim HS and Gius D. SIRT3 is a mitochondrial tumor suppressor: a scientific tale that connects aberrant cellular ROS, the Warburg effect, and carcinogenesis. Cancer Res 2012; 72: 2468-2472.

[13] Sack MN and Finkel T. Mitochondrial metabolism, sirtuins, and aging. Cold Spring Harb Perspect Biol 2012; 4: a013102.

[14] Scher MB, Vaquero A and Reinberg D. SirT3 is a nuclear NAD+-dependent histone deacetylase that translocates to the mitochondria upon cellular stress. Genes Deve 2007; 21: 920-928.

[15] Schwer B, North BJ, Frye RA, Ott M and Verdin E. The human silent information regulator (Sir) 2 homologue hSIRT3 is a mitochondrial nicotinamide adenine dinucleotide-dependent deacetylase. J Cell Biol 2002; 158: 647-657.

[16] Cooper HM, Huang JY, Verdin E and Spelbrink JN. A new splice variant of the mouse SIRT3 gene encodes the mitochondrial precursor protein. PLoS One 2009; 4: e4986.

[17] Desouki MM, Doubinskaia I, Gius D and Abdulkadir SA. Decreased mitochondrial SIRT3 expression is a potential molecular biomarker associated with poor outcome in breast cancer. Hum Pathol 2014; 45: 1071-1077.

[18] Marfe G, Tafani M, Indelicato M, Sinibaldi-Salimei P, Reali V, Pucci B, Fini M and Russo MA. Kaempferol induces apoptosis in two different cell lines via Akt inactivation, Bax and SIRT3 activation, and mitochondrial dysfunction. J Cell Biochem 2009; 106: 643-650.

[19] Liu Y, Liu YL, Cheng W, Yin XM and Jiang B. The expression of SIRT3 in primary hepatocellular carcinoma and the mechanism of its tumor suppressing effects. Eur Rev Med Pharmacol Sci 2017; 21: 978-998.

[20] Zhang B, Qin L, Zhou CJ, Liu YL, Qian HX and He SB. SIRT3 expression in hepatocellular carcinoma and its impact on proliferation and invasion of hepatoma cells. Asian Pac J Trop Med 2013; 6: 649-652.

[21] Wang JX, Yi Y, Li YW, Cai XY, He HW, Ni XC, Zhou J, Cheng YF, Jin JJ, Fan J and Qiu SJ. Down-regulation of sirtuin 3 is associated with poor prognosis in hepatocellular carcinoma after resection. BMC Cancer 2014; 14: 297.

[22] Allison SJ and Milner J. SIRT3 is pro-apoptotic and participates in distinct basal apoptotic pathways. Cell Cycle 2007; 6: 2669-2677.

[23] Li S, Banck M, Mujtaba S, Zhou MM, Sugrue MM and Walsh MJ. p53-induced growth arrest is regulated by the mitochondrial SirT3 deacetylase. PLoS One 2010; 5: e10486.

[24] Finley LW, Carracedo A, Lee J, Souza A, Egia A, Zhang J, Teruya-Feldstein J, Moreira PI, Cardoso SM, Clish CB, Pandolfi PP and Haigis MC. SIRT3 opposes reprogramming of cancer cell metabolism through HIF1α destabilization. Cancer Cell 2011; 19: 416-428.
[25] Dong XC, Jing LM, Wang WX and Gao YX. Downregulation of SIRT3 promotes ovarian carcinoma metastasis. Biochemi Biophys Res Commun 2016; 475: 245-250.
[26] Musgrove EA, Lee C, Buckley MF and Sutherland RL. Cyclin D1 induction in breast cancer cells shortens G1 and is sufficient for cells arrested in G1 to complete the cell cycle. Proc Natl Acad Sci U S A 1994; 91: 8022-8026.
[27] Li T, Kon N, Jiang L, Tan M, Ludwig T, Zhao Y, Baer R and Gu W. Tumor suppression in the absence of p53-mediated cell-cycle arrest, apoptosis, and senescence. Cell 2012; 149: 1269-1283.
[28] Chen J. The cell-cycle arrest and apoptotic functions of p53 in tumor initiation and progression. Cold Spring Harb Perspect Med 2016; 6: a026104.
[29] Tang Y, Luo J, Zhang W and Gu W. Tip60-dependent acetylation of p53 modulates the decision between cell-cycle arrest and apoptosis. Mol Cell 2006; 24: 827-839.
[30] Tang D, Wu D, Hirao A, Lahti JM, Liu L, Mazza B, Kidd VJ, Mak TW and Ingram AJ. ERK activation mediates cell cycle arrest and apoptosis after DNA damage independently of p53. J Biol Chem 2002; 277: 12710-12717.
[31] Zhang K, Wang L, Chen H, Shi Y, Liu Y, Liu J, Hong X and Liu JP. Pulmonary alveolar stem cells undergo senescence, apoptosis and differentiation by p53-dependent and-independent mechanisms in telomerase deficient mice. Clin Exp Pharmacol Physiol 2021; 48: 651-659.
[32] Pi H, Xu S, Reiter RJ, Guo P, Zhang L, Li Y, Li M, Cao Z, Tian L, Xie J, Zhang R, He M, Lu Y, Liu C, Duan W, Yu Z and Zhou Z. SIRT3-SOD2-mROS-dependent autophagy in cadmium-induced hepatotoxicity and salvage by melatonin. Autophagy 2015; 11: 1037-1051.
[33] Zhai M, Li B, Duan W, Jing L, Zhang B, Zhang M, Yu L, Liu Z, Yu B, Ren K, Gao E, Yang Y, Liang H, Jin Z and Yu S. Melatonin ameliorates myocardial ischemia reperfusion injury through SIRT 3-dependent regulation of oxidative stress and apoptosis. J Pineal Res 2017; 63: e12419.
[34] Galli U, Mesenzani O, Coppo C, Sorba G, Canonico PL, Tron GC and Genazzani AA. Identification of a sirtuin 3 inhibitor that displays selectivity over sirtuin 1 and 2. Eur J Med Chem 2012; 55: 58-66.
[35] Satoh K, Nagai F, Ushiyama K and Kano I. Specific inhibition of Na+, K(+)-ATPase activity by atractylon, a major component of Byaku-jutsu, by interaction with enzyme in the E2 state. Biochem Pharmacol 1996; 51: 339-343.
[36] Cheng Y, Mai JY, Hou TL, Ping J and Chen JJ. Antiviral activities of atractylon from atractylodis rhizoma. Mol Med Rep 2016; 14: 3704-3710.
[37] Chen LG, Jan YS, Tsai PW, Norimoto H, Michihara S, Murayama C and Wang CC. Anti-inflammatory and antinociceptive constituents of Atractylodes japonica Koidzumi. J Agric Food Chem 2016; 64: 2254-2262.
[38] Yu S, Yasukawa K and Takido M. Atractylodis Rhizoma extract and its component, atractylon, inhibit tumor promotion in mouse skin two-stage carcinogenesis. Phytomedicine 1994; 1: 55-58.
[39] Lai CC, Lin PM, Lin SF, Hsu CH, Lin HC, Hu ML, Hsu CM and Yang MY. Altered expression of SIRT gene family in head and neck squamous cell carcinoma. Tumor Biol 2013; 34: 1847-1854.

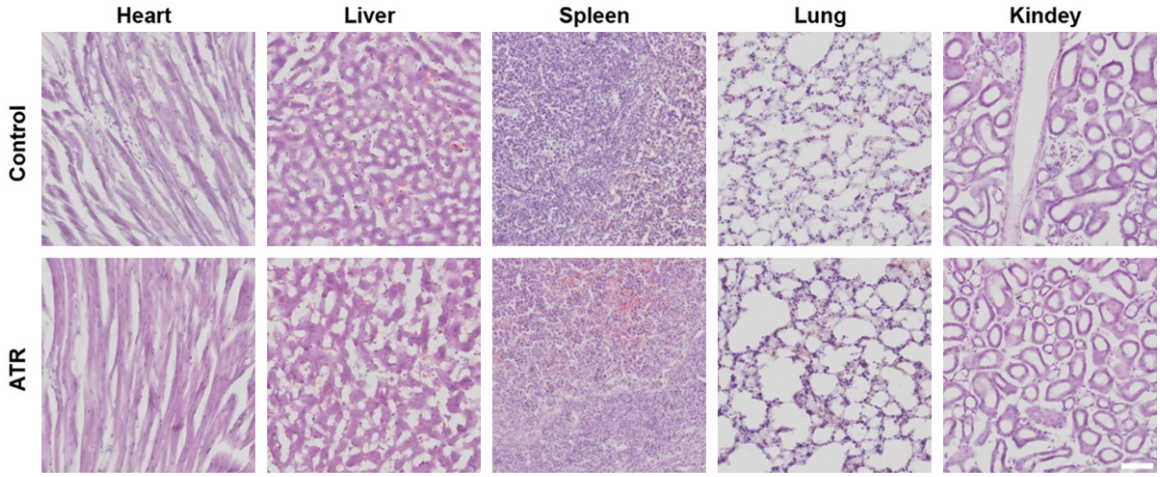

Supplementary Figure 1. HE staining of tissues from C6 xenograft mice. HE staining results of tissue sections of major organs from C6 xenograft mice treated with control or atractylon. Scale bar, 50 μm.